# Laser opacity in underdense preplasma of solid targets due to quantum electrodynamics effects

W.-M. Wang,[1,2,3,*] P. Gibbon,[4,5] Z.-M. Sheng,[6,7,3] Y.-T. Li,[1,3,8,†] and J. Zhang[7,3]

[1]*Beijing National Laboratory for Condensed Matter Physics, Institute of Physics, CAS, Beijing 100190, China*

[2]*Beijing Advanced Innovation Center for Imaging Technology, Department of Physics, Capital Normal University, Beijing 100048, China*

[3]*IFSA Collaborative Innovation Center, Shanghai Jiao Tong University, Shanghai 200240, China*

[4]*Forschungzentrum Jülich GmbH, Institute for Advanced Simulation, Jülich Supercomputing Centre, D-52425 Jülich, Germany*

[5]*Centre for Mathematical Plasma Astrophysics, Katholieke Universiteit Leuven, B-3000 Leuven, Belgium*

[6]*SUPA, Department of Physics, University of Strathclyde, Glasgow G4 0NG, United Kingdom*

[7]*Key Laboratory for Laser Plasmas (MoE) and Department of Physics and Astronomy, Shanghai Jiao Tong University, Shanghai 200240, China*

[8]*School of Physical Sciences, University of Chinese Academy of Sciences, Beijing 100049, China*

(Received 1 December 2016; published 5 July 2017)

We investigate how next-generation laser pulses at 10–200 PW interact with a solid target in the presence of a relativistically underdense preplasma produced by amplified spontaneous emission (ASE). Laser hole boring and relativistic transparency are strongly restrained due to the generation of electron-positron pairs and $\gamma$-ray photons via quantum electrodynamics (QED) processes. A pair plasma with a density above the initial preplasma density is formed, counteracting the electron-free channel produced by hole boring. This pair-dominated plasma can block laser transport and trigger an avalanchelike QED cascade, efficiently transferring the laser energy to the photons. This renders a 1-$\mu$m scale-length, underdense preplasma completely opaque to laser pulses at this power level. The QED-induced opacity therefore sets much higher contrast requirements for such a pulse in solid-target experiments than expected by classical plasma physics. Our simulations show, for example, that proton acceleration from the rear of a solid with a preplasma would be strongly impaired.

DOI: 10.1103/PhysRevE.96.013201

## I. INTRODUCTION

Current developments in ultraintense pulsed laser technology indicate that laser pulses at the 100-PW level will be available in the near future. A number of laboratories worldwide are pursuing this high power frontier, such as the European ELI to deliver 100–200 PW laser pulses [1], American OMEGA EP-OPAL for 100-PW pulses [2], and Russian XCELS for 200-PW pulses [3]. Interactions of such ultrarelativistic pulses with matter will likely enter a quantum electrodynamics (QED)-dominant regime. The plasma electrons can be instantly accelerated up to Lorentz factors $\gamma \sim a_0 > 1000$, where $a_0$ is the laser field strength normalized by $m_e c\omega_0/e$ and $\omega_0$ is the laser frequency. The QED parameter [4,5] of $\chi_e \simeq \gamma F_\perp/(eE_S)$ will easily exceed 1, so that abundant $\gamma$ photons should be generated via nonlinear Compton scattering, potentially offering an ultraintense $\gamma$-photon source [6,7]. Here, $E_S = 1.32\times10^{18}$ V/m is the Schwinger field [8,9] and $F_\perp$ is the transverse component of the Lorentz force. The generated photons of high energy under an ultrarelativistic laser field, with a QED parameter of photons [4,5] $\chi_{\rm ph} \simeq (\hbar\omega/m_e c^2)F_\perp/(eE_S)$ approaching or exceeding 1, will strongly trigger a Breit-Wheeler process and create electron-positron pairs in an avalanchelike way [10–13], which can present a laser intensity upper limit that is attainable [11,12] in the vacuum. This also provides a new approach for pair source generation [14–18].

On the other hand, when such a laser pulse is applied in a solid-target experiment, a preplasma produced by amplified spontaneous emission (ASE) could become more unavoidable [19,20] than the currently available case with a relatively low intensity pulse. For example, as low as $10^{-11}$ ASE of a pulse at $10^{21}$ W cm$^{-2}$ can produce a low level of preplasma ahead of a solid target [19,20], which can be ignored in most cases. For a pulse at $10^{23}$–$10^{25}$ W cm$^{-2}$, the same level of ASE (harder to achieve in technology) can produce a significant level of preplasma [19,20]. Due to the preplasma production, it will be a challenge to apply an extremely intense pulse in some applications based on laser interactions with solid-density targets, such as ion acceleration via radiation pressure [21–26], high-order harmonic and attosecond pulse generation [27–29], surface plasmon resonance [30–32], etc. Therefore, it is important to understand and anticipate the effects of a preplasma when a tightly focused pulse at 10–200 PW irradiates a solid target, where the above-mentioned QED effects are expected to dominate.

In this paper, we show that the QED effects can cause nearly complete energy depletion of such a pulse in a relativistically underdense, small-scale preplasma. This contrasts to the regime studied to date where the preplasma is actually rendered more transparent with increasing laser intensity because of laser hole boring and relativistic self-induced transparency [33]. At an early stage in the interaction, laser hole boring acts within the leading edge of the pulse: Electrons are pushed away from the peak laser intensity zone by a ponderomotive force and an electron-free channel is formed in the preplasma. Under the combined charge-separation field and the ponderomotive force, oscillating electrons leave the peak intensity zone and cause abundant $\gamma$-photon generation, which cools the electrons and reduces the relativistic transparency. Later, large numbers of pairs are created around the zone of peak laser intensity, which fill the preplasma-ion channel. The pair plasma can

*weiminwang1@126.com

†ytli@iphy.ac.cn

 

have a density much higher than the initial preplasma, which completely hinders further laser hole boring. This pair plasma strongly absorbs the laser energy and effectively transfers the energy to photons via a QED cascade [10–13]. In some cases, the pair-plasma density can be even higher than the relativistic critical density [13,17,33], and hence the pulse is strongly reflected, which could enhance the QED cascade together with the incident pulse. The QED-induced inflation of the preplasma implies that significant improvements in laser contrast technology will be necessary before pulses with these intensities can be used in solid-target experiments. In particular, only a small fraction of the laser energy is finally absorbed by plasma electrons, which may significantly limit the applications based on electrons preaccelerated by lasers, such as ion acceleration and neutron sources.

## II. PIC SIMULATION RESULTS

Our investigation is performed through particle-in-cell (PIC) simulations with the two-dimensional (2D) version of the KLAPS code [34,35], in which $\gamma$-photon and pair creation via QED effects is included. Our QED-PIC code has been fully benchmarked, as shown in Ref. [35] and the Supplemental Material [36]. A laser pulse is incident along the $+x$ direction with linear polarization along the $y$ direction, wavelength 1 $\mu$m (or the period $\tau_0 = 2\pi/\omega_0 = 3.33$ fs), and duration 30 fs of full width at half maximum. Its peak power $P_0$ is 200 PW ($P_0$ from 10 to 180 PW will be also taken in the simulations below) and peak amplitude $a_0 = 3049$. We take a fully tight laser focusing with a spot radius $r_0 = 1$ $\mu$m and a Gaussian distribution in intensity as generated in experiments [37], which could not follow the paraxial approximation [38]. A 0.5-$\mu$m-thick gold foil is taken, which is assumed to be composed of $Au^{+10}$ ions and electrons with a density of $530n_c$ ($n_c = 1.1\times10^{21}$ cm$^{-3}$) since we consider extremely intense pulses (a case with $Au^{+15}$ ions and a higher electron density will be discussed below). In front of the foil there is a preplasma with an exponential density profile of a scale length $L = 1$ $\mu$m ($L$ changing from 0.1 to 0.9 $\mu$m will also be taken below), which is expected to be produced by the laser ASE. Here, we use a thin foil since we focus on the laser absorption in the preplasma, which does not depend on the foil thickness. A simulation box size 82 $\mu$m $\times$ 80 $\mu$m in the $x\times y$ directions is taken. A fourth-order algorithm is employed for the current calculation [34,39], with which the noise is well controlled. We take the cell size in both the $x$ and $y$ directions as 0.0208 $\mu$m, the timestep as 0.0347 fs, and 16 electrons and ions per cell. An adjustable timestep is taken to calculate photon and pair generation, as described in the Supplemental Material [36]. Because the particle number is not large initially, memory overflow is avoided in our simulations. The absorption budget of laser energy into the various kinds of particles is closely monitored during the simulation.

### A. Impact of QED-induced opacity on proton acceleration

The red dashed line in Fig. 1(a) is the simulation result without the QED effects. It shows that due to laser hole boring and relativistic transparency, the 200-PW laser pulse with $a_0 = 3049$ easily penetrates through the preplasma with an

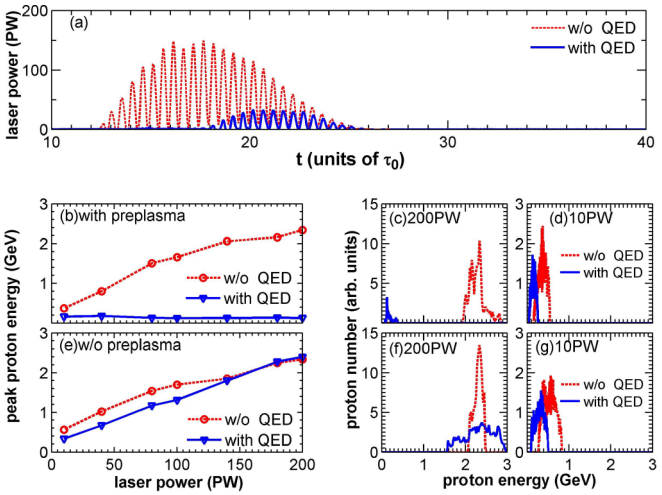


FIG. 1. (a) Temporal profile of the laser power passing through the preplasma rear. In (a)–(f), the red dashed line and the blue solid line correspond to the simulations without and with the QED effects, respectively. (b), (e) Peak energy of the protons at $80\tau_0$ vs the laser power. (c), (d), (f), (g) Proton energy spectra at $80\tau_0$ with different laser powers. (b)–(d) are the results with a foil with a preplasma. (e)–(g) are the results with a polished foil without a preplasma.

average density $66n_c \ll a_0n_c$ and a size of 8 $\mu$m, retaining most of its initial energy. However, the pulse loses nearly all energy in the same preplasma if the QED effects are included, as seen in the blue line in Fig. 1(a). Only 8% initial laser energy (with 30-PW peak power) is transported through the preplasma; without the QED effects, the value is 65% (with 150-PW peak power).

The large difference in laser energy depletion in the preplasma results in a quite different proton acceleration [Figs. 1(b) and 1(c)], where a 0.05-$\mu$m-thick proton layer of $50n_c$ is located in the rear of the gold foil and the layer is 2 $\mu$m wide in the $y$ direction. The protons are accelerated to a peak energy of about 2.4 GeV at $80\tau_0$ without the QED effects (note that we have not optimized target parameters for proton acceleration). With the QED effects, the peak energy is reduced to 0.13 GeV because the depleted laser energy is mainly transferred to photons [Fig. 2(a)], which do not contribute to proton acceleration. As the laser power is decreased [Figs. 1(d) and 1(b)], the difference in the proton energy is lessened between the two cases with and without the QED effects, since QED-induced depletion is weakened. The protons are accelerated mainly via target normal sheath acceleration (TNSA) [40] since nearly all the energy of the pulse at 10–200 PW is depleted in the preplasma with the QED effects (as discussed below). Without the QED effects, TNSA and radiation pressure acceleration work together since much laser energy is transported to the foil front.

In contrast to the results in Fig. 1(b) with the preplasma, Fig. 1(e) shows that the peak energy is continuously enhanced when a polished foil *without* the preplasma is taken. In this case, the peak energy shows little difference from the case without the QED effects. This is because when the foil is thin enough, the reaction of the foil to the pulse is weak and stays within a limited space, e.g., via the charge-separation

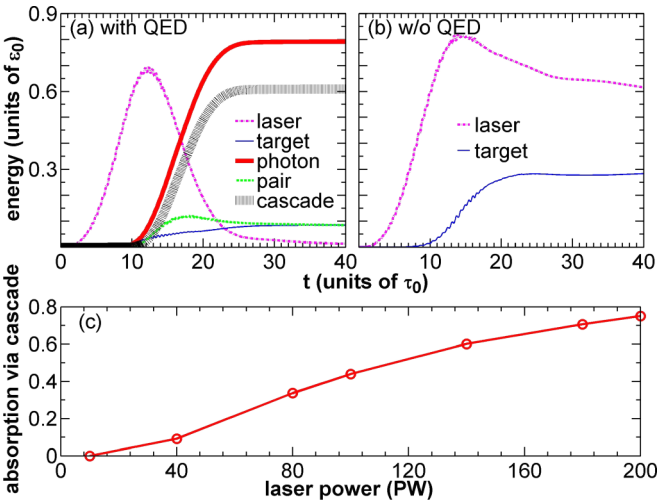


FIG. 2. (a), (b) Temporal evolution of residual energies of the laser pulse, target particles, photons, pairs, and the photons generated via the cascade (or only via the pairs), normalized by the total laser energy $\varepsilon_0$, where the laser power is taken as 200 PW. (a) and (b) correspond to the simulations with and without the QED effects, respectively. All particles exiting the simulation box are recorded and counted while the laser energy transported away is not counted. (c) Absorbed laser energy via the cascade in the preplasma region vs laser powers, where the energy is normalized by the total laser energy absorbed in this region.

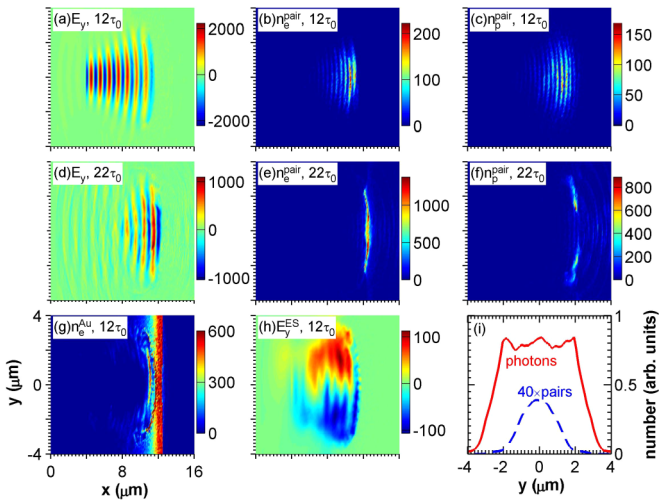


FIG. 3. Snapshots of (a), (d) laser electric fields $eE_y/m_e\omega_0 c$, (b), (e) pair-plasma electron densities $n_e^{\rm pair}/n_c$, (c), (f) positron densities $n_p^{\rm pair}/n_c$ at different times, (g) Au-target electron density $n_e^{\rm Au}/n_c$, and (h) electrostatic field $eE_y^{\rm ES}/m_e\omega_0 c$, where the maximum value is suppressed in (g) for clarity. (i) Number of generated photons and pairs vs their transverse position $y$, where the pair number is scaled by a factor of 40.

field. In this case the foil electrons are mainly accelerated along the laser propagation direction, which is less effective in triggering nonlinear Compton scattering for photon generation [see $\chi_e \simeq \gamma F_\perp/(eE_S)$ [4,5]]. Therefore, high energy protons and ions could be generated by 100-PW-class pulses, provided the laser contrast is sufficiently high and a thin enough foil is used. To optimize such proton and ion acceleration, one could match the foil thickness and the laser power as was done in Ref. [41], but only after taking QED effects into account. Besides, we find that when a circularly polarized pulse is taken, the QED effects at a high power also significantly impact the proton acceleration from the foil either with or without a preplasma, although at a relatively low power (e.g., 10 PW) the impact can be ignored with a polished foil, as shown in Ref. [42]. Some results with circularly polarized pulses can be found in the Supplemental Material [36].

### B. QED-induced laser depletion in underdense preplasma

In Fig. 2(a) the relative contributions of the generated photons and pairs, and the target particles (mainly the preplasma) to the laser energy depletion with a laser power of 200 PW are shown. About 80% laser energy is finally transferred to the $\gamma$ photons. First, some photons are generated around the laser axis at $y = 0$ [Fig. 3(i)] via nonlinear Compton scattering of the preplasma electrons after being accelerated by the pulse. The generated photons trigger the Breit-Wheeler process and create pairs in the peak laser intensity zone around the laser axis [Fig. 3(i)]. Likewise, the pairs under the laser fields also generate nonlinear Compton photons. In this way, an avalanchelike cascade is formed, causing copious photon generation. According to the black dashed line in Fig. 2(a), 77% of the photons are generated via the pairs (or via the cascade) and the other 23% via the preplasma electrons. Therefore, the pairs or the cascade dominate photon generation and laser energy absorption over the preplasma electrons.

There are two reasons for the cascade dominating the laser absorption. First, the positrons, unlike massive ions, can be easily accelerated to ultrarelativistic energies and can thus contribute to the photon generation basically to the same extent as the electrons; they can also inhibit the acceleration of ions and protons. Second, due to the requirement of the QED parameter $\chi_{\rm ph} \simeq (\hbar\omega/m_e c^2)F_\perp/(eE_S)$ approaching or exceeding 1 [4,5] for the strong creation of pairs, most pairs are created in the peak laser intensity zone around the laser axis [Figs. 3(i), 3(b), and 3(c)], basically where the photon generation rate is the highest. By contrast, the preplasma electrons are expelled away from this peak intensity zone [Fig. 3(g)] via laser hole boring, within the pulse leading edge but mainly before the pair creation. This causes the reduction of photon generation via the preplasma electrons.

Due to the expelled electrons, a strong charge-separation field is formed around the laser axis [Fig. 3(h)], which tends to keep the pair electrons within this region. Under this field, many freshly created pair electrons remain localized, leading to a growing pair-plasma electron density around the laser axis: It reaches about $1400n_c$ at $22\tau_0$ [Figs. 3(e) and 3(b)]. Note that the charge-separation field also ensures that the positron densities are always lower than the pair-plasma electron densities [Figs. 3(c) and 3(f)]. In this way, the pair plasma fills the preplasma-electron-free channel and its density is much higher than the initial preplasma density, as seen in Figs. 3(g), 3(b), 3(c), and 3(e). Then, the laser hole boring and relativistic transparency can be completely inhibited. Note that the charge-separation field is formed before the cascade development, as shown in Fig. S5 in

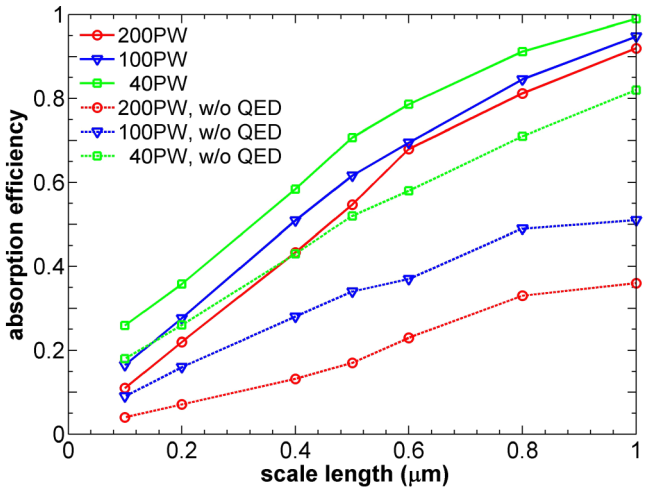


FIG. 4. The energy absorption efficiency of lasers with different powers in the preplasma region vs preplasma density scale lengths $L$.

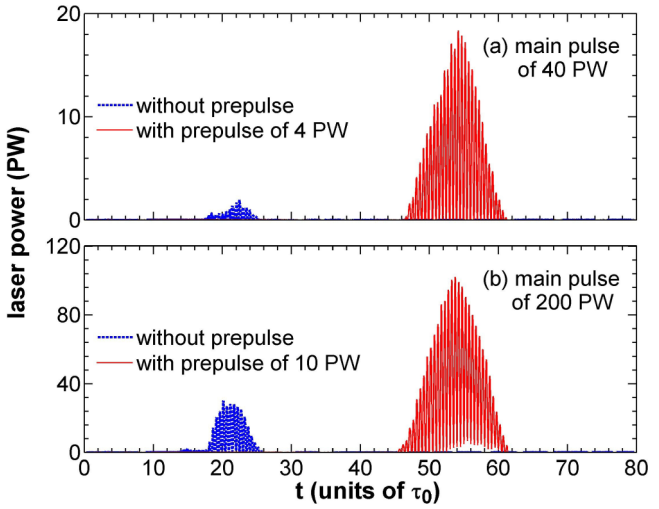


FIG. 5. Temporal profile of laser power passing through the preplasma rear, where a controlled prepulse is taken 120 fs ahead of the main pulse in the red line and no prepulse is taken in the blue dashed line. (a) A 40-PW main pulse and a 4-PW prepulse are adopted. (b) A 200-PW main pulse and a 10-PW prepulse are adopted.

the Supplemental Material [36]. This charge-separation field significantly changes particle motion under the laser field and enhances the QED effects [7]. Without it, preplasma electrons will be along the laser propagation direction and the QED parameters of the electrons will approach zero. This is different from the counterpropagating laser geometry [10–13,15–18], since in our case the plasma composed of a preplasma and pairs is relativistically underdense at most times (before $22\tau_0$) and the reflection is weak. As the pulse strength $a_0$ is strongly reduced [Fig. 3(d)], the density can be even higher than $a_0 n_c$ [Fig. 3(e)], which causes the pulse to be significantly reflected. Both the reflected and incident pulses can be quickly absorbed since they can strengthen the QED cascade [12,13].

The contribution of the QED cascade to the laser depletion is weakened with decreasing laser power [Fig. 2(c)]. In this figure, we plot the laser absorption via the cascade (or only via the pairs). When the power is decreased to 100 PW from 200 PW, the contribution of the pairs to the laser absorption is reduced to 44% from 75% (note that a relativistically overdense foil slab can absorb the pulse as efficiently as in our case with a relativistically underdense preplasma, but less contribution comes from the cascade since the foil electrons and ions gain more laser energy [43]). The value is further reduced to about 10% at 40 PW. Therefore, in a 1-$\mu$m scale-length preplasma, the cascade starts to be important at 40 PW and becomes the leading effect at around 100 PW.

To gauge the sensitivity of this result to the initial preplasma density scale length $L$ and the laser power, a limited parameter scan of absorption efficiencies is depicted in Fig. 4, about which one can make several observations. First, one can see that QED effects generally result in a much higher laser absorption for powers of 40–200 PW across the whole range of scale lengths considered ($L = 0.1$–$1.0$ $\mu$m). Hence, a much higher laser contrast will be required to apply such a pulse in future experiments than expected by classical plasma physics. The contrast between the two cases with and without the QED effects is reduced for lower powers, but the difference is still apparent even for relatively sharp profiles with $L = 0.1$ $\mu$m. Second, with a smaller $L$ (or a higher laser contrast) and a given power, less laser energy is depleted in the preplasma since the laser preplasma interaction zone is decreased. Third, with a lower power and a given $L$, the absorption efficiency of the laser energy is higher. This is because the reaction of the preplasma to the lower-power pulse is comparatively stronger, i.e., a higher ratio of charge-separation field strength to the pulse strength and relatively more photons generated via the preplasma electrons, even though fewer photons are generated via the pairs or the cascade. To get 50% of the laser energy transported to the solid-target front behind the preplasma, according to Fig. 4, $L$ should be around 0.5 $\mu$m for the 200-PW pulse, and $L \simeq 0.4$ $\mu$m for the 100- and 40-PW pulses. When the $Au^{+10}$ target is replaced by an $Au^{+15}$ target, the laser depletion in the preplasma becomes stronger, as seen in our simulations. This is because the $Au^{+15}$ target and its preplasma with the same $L$ have higher electron densities or more electrons.

### C. Reduction of QED-induced opacity via a controlled prepulse

QED-induced preplasma inflation and the hinderance of the laser passage to the solid-target surface can be mitigated by using a controlled prepulse. When the prepulse is ahead of the main one, it can create a nearly-electron-free channel in the preplasma, reducing the interaction of the main pulse with the preplasma electrons and consequently weakening the QED effects. In our simulations, the prepulse and main pulse have the same duration of 30 fs and spot radius $r_0 = 1$ $\mu$m and an $Au^{+10}$ target with a preplasma of $L = 1$ $\mu$m is employed. In Fig. 5(a), when a 4-PW prepulse is taken, the 40-PW main pulse is transported through the preplasma with 18 times more energy (up to 36% initial energy of the main pulse) than the case without a prepulse. In Fig. 5(b), when a 10-PW prepulse is taken, the 200-PW main pulse is transported through the preplasma with six times more energy (up to 47% initial energy of the main pulse) than the case without a prepulse.

Several works took QED-PIC simulations to investigate the laser-foil interactions at the 100-PW level [43–45] and 10-PW level [6,7], respectively. However, a preplasma was not included [44,45] or was considered to be unimportant [6,7,43]. Even though our results are obtained according to 2D simulations, it is expected that they are still valid in three-dimensional (3D) geometry, since particles should mainly move in the $x$-$y$ plane with a linearly polarized, ultrahigh intensity pulse. Grismayer *et al.* showed that 2D and 3D simulations can give very close results on the QED cascade development driven by linearly polarized pulses [18].

## III. SUMMARY

In summary, we have shown by PIC simulations that the QED effects can significantly enhance the opacity of a laser pulse at 10–200 PW in a relativistically transparent preplasma, which is produced by ASE nearly unavoidable. This contrasts to the expectation according to classical laser-plasma physics that such a preplasma is not important for an ultrahigh intensity pulse and it is rendered more transparent with increasing laser intensity because of laser hole boring and relativistic self-induced transparency. Our simulations show that a 1-$\mu$m scale-length preplasma is completely opaque for such a pulse. To achieve transparencies above 50%, a preplasma with a scale length below 0.4 $\mu$m is required. Therefore, the QED-induced opacity sets much higher demands on laser contrast technology for pulse powers of 10–200 PW than expected by classical plasma physics. We have illustrated that ahead of the main pulse, a controlled prepulse can effectively reduce such opacity, even if the prepulse power is far below the main pulse power.

The QED-induced opacity is most potent when a high-density pair plasma is formed around the peak laser intensity zone, to fill a preplasma-electron-free channel produced via laser hole boring. The pair plasma triggers an avalanchelike QED cascade to strongly absorb the laser energy, which finally transfers to photons. The cascade becomes the leading depletion mechanism and dominates over the depletion by preplasma electrons when the pulse power reaches 100 PW. It starts to be significant at 40 PW. Below 40 PW, the laser energy is depleted mainly due to purely nonlinear Compton scattering via preplasma electrons. In any case, little laser energy is finally transferred to the electrons of either the preplasma or the pairs, which will significantly affect the applications based on electrons preaccelerated by laser pulses, e.g., ion acceleration.

## ACKNOWLEDGMENTS

This work was supported by the National Basic Research Program of China (Grant No. 2013CBA01500), NSFC (China) (Grants No. 11375261, No. 11421064, No. 11374210, and No. 113111048), Science Challenge Project of China (Grant No. TZ2016005), and the Strategic Priority Research Program of the Chinese Academy of Sciences (Grants No. XDB16010200 and XDB07030300). Z.M.S. acknowledges the support of a Leverhulme Trust Research Grant and EPSRC (UK) Grant No. EP/N028694/1. The authors gratefully acknowledge the computing time granted by the JARA-HPC Vergabegremium and VSR commission provided on the JARA-HPC Partition part of the supercomputer JUQUEEN at Forschungszentrum Jülich.

[1] http://www.extreme-light-infrastructure.eu
[2] J. D. Zuegel, Technology development and prospects for 100-PW-class optical parametric chirped-pulse amplification pumped by OMEGA EP, plenary talk at the 2nd International Symposium on High Power Laser Science and Engineering (HPLSE 2016), March 15–18, 2016, Suzhou, China (unpublished).
[3] http://www.xcels.iapras.ru/
[4] T. Erber, Rev. Mod. Phys. **38**, 626 (1966).
[5] N. V. Elkina, A. M. Fedotov, I. Yu. Kostyukov, M. V. Legkov, N. B. Narozhny, E. N. Nerush, and H. Ruhl, Phys. Rev. ST Accel. Beams **14**, 054401 (2011).
[6] C. P. Ridgers, C. S. Brady, R. Duclous, J. G. Kirk, K. Bennett, T. D. Arber, A. P. L. Robinson, and A. R. Bell, Phys. Rev. Lett. **108**, 165006 (2012).
[7] C. S. Brady, C. P. Ridgers, T. D. Arber, A. R. Bell, and J. G. Kirk, Phys. Rev. Lett. **109**, 245006 (2012).
[8] F. Sauter, Z. Phys. **69**, 742 (1931).
[9] J. Schwinger, Phys. Rev. **82**, 664 (1951).
[10] A. R. Bell and J. G. Kirk, Phys. Rev. Lett. **101**, 200403 (2008).
[11] A. M. Fedotov, N. B. Narozhny, G. Mourou, and G. Korn, Phys. Rev. Lett. **105**, 080402 (2010).
[12] S. S. Bulanov, T. Zh. Esirkepov, A. G. R. Thomas, J. K. Koga, and S. V. Bulanov, Phys. Rev. Lett. **105**, 220407 (2010).
[13] E. N. Nerush, I. Y. Kostyukov, A. M. Fedotov, N. B. Narozhny, N. V. Elkina, and H. Ruhl, Phys. Rev. Lett. **106**, 035001 (2011).
[14] I. V. Sokolov, N. M. Naumova, J. A. Nees, and G. A. Mourou, Phys. Rev. Lett. **105**, 195005 (2010).
[15] M. Lobet, C. Ruyer, A. Debayle, E. d'Humieres, M. Grech, M. Lemoine, and L. Gremillet, Phys. Rev. Lett. **115**, 215003 (2015).
[16] V. F. Bashmakov, E. N. Nerush, I. Yu. Kostyukov, A. M. Fedotov, and N. B. Narozhny, Phys. Plasmas **21**, 013105 (2014).
[17] T. Grismayer, M. Vranic, J. L. Martins, R. A. Fonseca, and L. O. Silva, Phys. Plasmas **23**, 056706 (2016).
[18] T. Grismayer, M. Vranic, J. L. Martins, R. A. Fonseca, and L. O. Silva, Phys. Rev. E **95**, 023210 (2017).
[19] B. Dromey, S. Kar, M. Zepf, and P. Foster, Rev. Sci. Instrum. **75**, 645 (2004).
[20] O. Lundh, F. Lindau, A. Persson, C.-G. Wahlstrom, P. McKenna, and D. Batani, Phys. Rev. E **76**, 026404 (2007).
[21] T. Esirkepov, M. Borghesi, S. V. Bulanov, G. Mourou, and T. Tajima, Phys. Rev. Lett. **92**, 175003 (2004).
[22] X. Q. Yan, C. Lin, Z. M. Sheng, Z. Y. Guo, B. C. Liu, Y. R. Lu, J. X. Fang, and J. E. Chen, Phys. Rev. Lett. **100**, 135003 (2008).
[23] A. P. L. Robinson, M. Zepf, S. Kar, R. G. Evans, and C. Bellei, New J. Phys. **10**, 013021 (2008).
[24] B. Shen, X. Zhang, Z. M. Sheng, M. Y. Yu, and J. Cary, Phys. Rev. ST Accel. Beams **12**, 121301 (2009).

[25] L. L. Yu, H. Xu, W. M. Wang, Z. M. Sheng, B. F. Shen, W. Yu, and J. Zhang, New J. Phys. **12**, 045021 (2010).
[26] F. L. Zheng, S. Z. Wu, H. C. Wu, C. T. Zhou, H. B. Cai, M. Y. Yu, T. Tajima, X. Q. Yan, and X. T. He, Phys. Plasmas **20**, 013107 (2013).
[27] S. V. Bulanov, N. M. Naumova, and F. Pegoraro, Phys. Plasmas **1**, 745 (1994).
[28] P. Gibbon, Phys. Rev. Lett. **76**, 50 (1996).
[29] U. Teubner and P. Gibbon, Rev. Mod. Phys. **81**, 445 (2009).
[30] S. Kahaly, S. Yadav, W.-M. Wang, S. Sengupta, Z. M. Sheng, A. Das, P. K. Kaw, and G. R. Kumar, Phys. Rev. Lett. **101**, 145001 (2008).
[31] W.-M. Wang, Z.-M. Sheng, and J. Zhang, Phys. Plasmas **15**, 030702 (2008).
[32] S. Monchoce, S. Kahaly, A. Leblanc, L. Videau, P. Combis, F. Reau, D. Garzella, P. D'Oliveira, Ph. Martin, and F. Quere, Phys. Rev. Lett. **112**, 145008 (2014).
[33] P. Gibbon, *Short Pulse Laser Interactions with Matter* (Imperial College Press, London, 2000).
[34] W.-M. Wang, P. Gibbon, Z.-M. Sheng, and Y.-T. Li, Phys. Rev. E **91**, 013101 (2015).
[35] W.-M. Wang, Z.-M. Sheng, P. Gibbon, and Y.-T. Li, arXiv:1608.06356.
[36] See Supplemental Material at http://link.aps.org/supplemental/10.1103/PhysRevE.96.013201, in which part one is on proton acceleration by a circularly polarized pulse, part two presents the scheme of an adjustable QED time step and a benchmark of KLAPS simulations against OSIRIS ones, and part three shows photon and pair generation with time.
[37] S.-W. Bahk, P. Rousseau, T. A. Planchon, V. Chvykov, G. Kalintchenko, A. Maksimchuk, G. A. Mourou, and V. Yanovsky, Opt. Lett. **29**, 2837 (2004).
[38] I. Thiele, S. Skupin, and R. Nuter, J. Comput. Phys. **321**, 1110 (2016).
[39] W.-M. Wang, P. Gibbon, Z.-M. Sheng, and Y.-T. Li, Phys. Rev. Lett. **114**, 015001 (2015).
[40] M. Borghesi, J. Fuchs, S. V. Bulanov, A. J. Mackinnon, P. K. Patel, and M. Roth, Fusion Sci. Technol. **49**, 412 (2006).
[41] T. Esirkepov, M. Yamagiwa, and T. Tajima, Phys. Rev. Lett. **96**, 105001 (2006).
[42] M. Tamburini, F. Pegoraro, A. Di Piazza, C. H. Keitel, and A. Macchi, New J. Phys. **12**, 123005 (2010).
[43] M. C. Levy, T. G. Blackburn, N. Ratan, J. Sadler, C. P. Ridgers, M. Kasim, L. Ceurvorst, J. Holloway, M. G. Baring, A. R. Bell, S. H. Glenzer, G. Gregori, A. Ilderton, M. Marklund, M. Tabak, S. C. Wilks, and P. A. Norreys, arXiv:1609.00389.
[44] P. Zhang, C. P. Ridgers, and A. G. R. Thomas, New J. Phys. **17**, 043051 (2015).
[45] I. Y. Kostyukov and E. N. Nerush, Phys. Plasmas **23**, 093119 (2016).